

# Tuning-Free Online Robust Principal Component Analysis through Implicit Regularization

Lakshmi Jayalal\*, Gokularam Muthukrishnan\*, Sheetal Kalyani\*

**Abstract**—The performance of Online Robust Principal Component Analysis (OR-PCA) technique heavily depends on the optimum tuning of the explicit regularizers. This tuning is dataset-sensitive and often impractical to optimize in real-world scenarios. We aim to remove the dependency on these tuning parameters by using implicit regularization. To this end, we develop an approach that integrates implicit regularization properties of various gradient descent methods to estimate sparse outliers and low-dimensional representations in a streaming setting—a non-trivial extension of existing techniques. A key novelty lies in the design of a new parameterization for matrix estimation in OR-PCA. Our method incorporates three different versions of modified gradient descent that separate but naturally encourage sparsity and low-rank structures in the data. Experimental results on synthetic and real-world video datasets demonstrate that the proposed method, namely, Tuning-Free OR-PCA (TF-ORPCA), outperforms existing OR-PCA methods. TF-ORPCA makes it more scalable for large datasets.

**Index Terms**—Online Robust PCA, Implicit regularization, Gradient Descent

## I. INTRODUCTION

Robust Principal Component Analysis (RPCA) [1] is an outlier-resilient linear dimensionality reduction method. Several RPCA techniques have been proposed [2]–[4]; with a detailed overview provided in [5]. In online settings where data arrive sequentially [6], Online Robust Principal Component Analysis (OR-PCA) recursively obtains principal components [7], [8], reducing the memory footprint and improving efficiency by processing data as it is acquired. Variants like online moving window RPCA (OMW-RPCA) use a sliding window [9], [10] for non-stationary environments. [11] demonstrates how OMW-RPCA can be applied to real-world moving target detection. Other online approaches exist, such as GRASTA [12], robust subspace tracking [13], and residual-based OR-PCA [14]. However, tuning regularization parameters poses significant practical hurdles for its widespread deployment. In this paper, we demonstrate that the dependency on regularization parameters can be alleviated through implicit regularization (IR) methods [15]–[21].

IR leverages implicit biases in carefully designed optimization algorithms to enhance model generalization without explicit regularization terms. For instance, gradient descent often converges toward well-generalizing solutions despite multiple local minima in overparameterized problems, acting as a form of IR [15], an effect further evident in techniques like early stopping and noise introduced by stochastic gradient descent

that help avoid overfitting and improve generalization [16], [17]. Interestingly, even the choice of optimization algorithm introduces IR. For example, in unconstrained, underdetermined least-squares problems, gradient descent reaches the minimum Euclidean norm solution [18], while its parameterized form with early stopping can lead to minimal  $\ell_1$ -norm solutions under certain conditions [19]. We introduce Tuning-Free OR-PCA (TF-ORPCA), a novel framework that integrates tailored IR techniques for each subproblem (including a new algorithm for the subspace basis, adapted sparse IR, and early-stopped Momentum Gradient Descent (MGD)), efficiently managing streaming data with sparse outliers by removing dependency on the explicit regularization parameter. Experimental validation on synthetic and real-world datasets demonstrates that TF-ORPCA outperforms existing OR-PCA techniques, achieving superior low-rank and outlier recovery by leveraging IR and fixed hyperparameters, as opposed to traditional OR-PCA methods.

**Basic notations:** Bold, lowercase letters denote vectors; bold, uppercase for matrices.  $\mathbf{X}^\top$  is the transpose of  $\mathbf{X}$ . Column  $\mathbf{z}_i$  of the data matrix  $\mathbf{Z}$  is the  $i$ -th data sample.  $\|\mathbf{X}\|_F$ ,  $\|\mathbf{X}\|_*$ , and,  $\|\mathbf{x}\|_p$  represent Frobenius, nuclear and  $\ell_p$  norm, respectively.  $\odot$  and  $\odot$  denote Hadamard power and Hadamard product, respectively.  $\mathbf{1}_w$  is a  $w$ -sized row vector of ones.

## II. OR-PCA

For the observed data  $\mathbf{Z} = \mathbf{X} + \mathbf{E}$ , where a sparse outlier  $\mathbf{E}$  corrupts  $\mathbf{X}$ , the PCP optimization problem is:

$$\min_{\mathbf{X}, \mathbf{E}} \frac{1}{2} \|\mathbf{Z} - \mathbf{X} - \mathbf{E}\|_F^2 + \lambda_1 \|\mathbf{X}\|_* + \lambda_2 \|\mathbf{E}\|_1, \quad (1)$$

where  $\mathbf{Z}, \mathbf{X}, \mathbf{E} \in \mathbb{R}^{p \times n}$  and  $\lambda_1, \lambda_2$  are the explicit parameters.

For sequential data, OR-PCA leverages bilinear decomposition of the low-rank matrix as  $\mathbf{X} = \mathbf{L}\mathbf{R}^\top$ , where  $\mathbf{L} \in \mathbb{R}^{p \times r}$  is the basis for the rank- $r$  subspace of  $\mathbf{X}$  and rows of  $\mathbf{R} \in \mathbb{R}^{n \times r}$  provide the corresponding coefficients. This provides a variational characterization of the nuclear norm as the infimum of the Frobenius norms of its factors when  $r$  is known [22]:

$$\|\mathbf{X}\|_* = \inf_{\mathbf{L} \in \mathbb{R}^{p \times r}, \mathbf{R} \in \mathbb{R}^{n \times r}} \left\{ \frac{1}{2} (\|\mathbf{L}\|_F^2 + \|\mathbf{R}\|_F^2) : \mathbf{X} = \mathbf{L}\mathbf{R}^\top \right\}. \quad (2)$$

In online data, let  $\mathbf{z}_t \in \mathbb{R}^{p \times 1}$  be the sample revealed at time  $t$ . For a slowly changing basis  $\mathbf{L}$ , the revealed sample can be expressed as  $\mathbf{z}_t = \mathbf{L}\mathbf{r}_t^\top + \mathbf{e}_t$ , where  $\mathbf{r}_t \in \mathbb{R}^{1 \times r}$  is its coefficient with respect to  $\mathbf{L}$  and the corresponding sparse outlier  $\mathbf{e}_t \in \mathbb{R}^{p \times 1}$ . This leads to the online reformulation:

$$\min_{\mathbf{L}, \{\mathbf{r}_t\}, \{\mathbf{e}_t\}} \frac{1}{n} \sum_{t=1}^n f(\mathbf{r}_t, \mathbf{e}_t, \mathbf{L}, \mathbf{z}_t) + \frac{\lambda_1}{2n} \|\mathbf{L}\|_F^2, \quad (3)$$

\*The authors are with the Department of Electrical Engineering, Indian Institute of Technology Madras, Chennai 600036, India (e-mail: {ee19d751@smail, ee17d400@smail, skalyani@ee}.iitm.ac.in)

where  $f(\mathbf{r}_t, \mathbf{e}_t, \mathbf{L}, \mathbf{z}_t) := \mathcal{L}_1(\mathbf{z}_t, \mathbf{L}\mathbf{r}_t, \mathbf{e}_t) + \frac{\lambda_1}{2}\|\mathbf{r}_t\|_2^2 + \lambda_2\|\mathbf{e}_t\|_1$  is the loss function and  $\mathcal{L}_1(\mathbf{z}_t, \mathbf{x}_t, \mathbf{e}_t) := \frac{1}{2}\|\mathbf{z}_t - \mathbf{x}_t - \mathbf{e}_t\|_F^2$ , the loss in data fidelity. OR-PCA employs alternating minimization to iteratively update  $P_1$ ,  $P_2$ , and  $P_3$  at each step  $t$ .

$$P_1 := \min_{\mathbf{e}_t \in \mathbb{R}^{p \times 1}} \mathcal{L}_1(\mathbf{z}_t, \mathbf{L}\mathbf{r}_t^\top, \mathbf{e}_t) + \lambda_2\|\mathbf{e}_t\|_1 \mid \{\mathbf{L}, \mathbf{r}_t\}, \quad (4)$$

$$P_2 := \min_{\mathbf{r}_t \in \mathbb{R}^{1 \times r}} \mathcal{L}_1(\mathbf{z}_t, \mathbf{L}\mathbf{r}_t^\top, \mathbf{e}_t) + \frac{\lambda_1}{2}\|\mathbf{r}_t\|_2^2 \mid \{\mathbf{L}, \mathbf{e}_t\}, \quad (5)$$

$$P_3 := \min_{\mathbf{L} \in \mathbb{R}^{p \times r}} \mathcal{L}_1(\mathbf{z}_t, \mathbf{L}\mathbf{r}_t^\top, \mathbf{e}_t) + \frac{\lambda_1}{2}\|\mathbf{L}\|_F^2 \mid \{\mathbf{e}_t, \mathbf{r}_t\}. \quad (6)$$

The quality of the estimates depends on the proper setting of  $\lambda_1$  and  $\lambda_2$ . These require data-dependent tuning via computationally expensive methods like grid search or cross-validation, often failing to generalize well to unseen data.

### III. TUNING-FREE OR-PCA

---

#### Algorithm 1 Tuning-Free OR-PCA

---

**Input**  $\mathbf{Z} = \mathbf{z}_1, \mathbf{z}_2, \dots, \mathbf{z}_T$ ,  $n$  - number of samples,  $r$  - intrinsic rank,  $p$  - ambient dimension,  $\mathbf{L}_0, \mathbf{r}_0, \mathbf{e}_0, \mathbf{g}_0 \in \mathbb{R}^{p \times 1}, \mathbf{v}_0 \in \mathbb{R}^{p \times r}$  - initial solutions,  $T_a \forall a \in \{r, e, L\}$  - number of epochs for each parameter  $\mathbf{r}_t, \mathbf{e}_t$  and  $\mathbf{L}$ ,  $T_0$  - max iterations for alternating optimization.

```

1: for  $t = 1$  to  $n$  do
2:   Reveal  $\mathbf{z}_t$ 
3:    $\mathbf{r}_0 = \mathbf{r}_{t-1}, \mathbf{e}_0 = \mathbf{e}_{t-1}, \mathbf{e}_t = \mathbf{e}_{t-1}$ 
4:   repeat
5:      $\mathbf{r}_t \leftarrow \text{MGD}(\mathbf{z}_t - \mathbf{e}_t, T_r)$ 
6:      $\mathbf{e}_t \leftarrow \text{HPGrad}(\mathbf{z}_t - \mathbf{L}_{t-1}\mathbf{r}_t, T_e)$ 
7:      $\epsilon \leftarrow \max \left\{ \frac{\|\mathbf{r}_t - \mathbf{r}_0\|_2}{\|\mathbf{z}_t\|_2}, \frac{\|\mathbf{e}_t - \mathbf{e}_0\|_2}{\|\mathbf{z}_t\|_2} \right\}$ 
8:      $k \leftarrow k + 1$ 
9:   until  $\epsilon < 10^{-3}$  or  $k = T_0$ 
10:   $\mathbf{L} = \text{HPGroupGrad}(\mathbf{z}_t - \mathbf{e}_t, \mathbf{r}_t, T_L, \mathbf{L})$ 
11:   $\mathbf{R}[t, :] = \mathbf{r}_t; \mathbf{E}[:, t] = \mathbf{e}_t^\top$ 
12: end for
13: return  $\mathbf{L}, \mathbf{R}, \mathbf{E}$ 
```

---

We utilize IR methods to individually address problems  $P_1$ ,  $P_2$ , and  $P_3$ , thus circumvent tuning  $\lambda_1$  and  $\lambda_2$ . Following [7], we alternately optimize  $P_1$  and  $P_2$  to estimate  $\mathbf{e}_t$  and  $\mathbf{r}_t$ , based on the previous  $\mathbf{L}$  estimate, until convergence.  $\mathbf{e}_t$  and  $\mathbf{r}_t$  then optimize  $P_3$ , updating  $\mathbf{L}$ . This process relies on the most recent estimates for each optimization problem. Crucially, adapting IR techniques for these specific subproblems within the OR-PCA framework requires a novel approach. The optimization for each sub-problem employs specific early stopping criteria, crucial for achieving IR. The precise stopping rule details for each algorithm are provided in the Appendix. The overall approach is summarized in Algorithm 1. In the following subsections, we discuss the solutions for each of these sub-optimization problems.

#### A. Estimating the sparse outlier $\mathbf{e}_t$

To estimate the sparse outlier  $\mathbf{e}_t$  (optimization problem  $P_1$  (equation (4))), we adopt a modified gradient descent

approach, as in [19], [23], which efficiently optimizes  $\ell_1$ -norm regularized solution for OR-PCA. This method involves decomposing the optimization parameter  $\mathbf{e}$  in each iteration  $i$ . Then, these decomposed parameters are iteratively updated, resulting in a multiplicative update (lines 4, 5 of Algorithm 2). This decomposition inherently drives many non-significant components towards 0, thereby implicitly inducing sparsity and eliminating the dependency on the parameter  $\lambda_2$ . The approach is summarized in Algorithm 2, where the residual  $\Delta$  updates the decomposed parameters  $\mathbf{m}$  and  $\mathbf{n}$ .

---

#### Algorithm 2 HPGrad( $\tilde{\mathbf{z}}_t, T_e$ )

---

```

1: Initialization:  $\alpha = 10^{-5}, \eta = 5 \times 10^{-3}, \mathbf{m} = \alpha \mathbf{1}_p,$   

    $\mathbf{n} = \alpha \mathbf{1}_p, \mathbf{e} = \mathbf{0}_p.$ 
2: for  $i = 0$  to  $T_e - 1$  do
3:    $\Delta \leftarrow \frac{4}{p}(\tilde{\mathbf{z}}_t - \mathbf{e})$ 
4:    $\mathbf{m} \leftarrow \mathbf{m} \odot (1 - \eta\Delta); \quad \mathbf{n} \leftarrow \mathbf{n} \odot (1 + \eta\Delta)$ 
5:    $\mathbf{e} \leftarrow \mathbf{m}^{\odot 2} - \mathbf{n}^{\odot 2}$ 
6: end for
7: return  $\mathbf{e}$ 
```

---

#### B. Estimating the Coefficient Vector $\mathbf{r}_t$

$P_2$  given in equation (5) is a ridge regression problem where  $\lambda_1$  controls the  $\ell_2$ -norm to estimate  $\mathbf{r}_t$ . We use vanilla MGD to estimate  $\mathbf{r}_t$ , motivated by its theoretical connection to  $\ell_2$ -regularization, established and explored in [20]. This suggests that MGD is a viable tuning-free alternative to  $\ell_2$ -regularization loss. The early stopping time  $T_r$  of vanilla MGD acts as an IR parameter, related to the ridge regression tuning parameter by  $\lambda = \frac{2}{T_r^2}$ . By setting  $T_r$ , we implicitly control the  $\ell_2$ -regularization, obviating  $\lambda_1$  from (5). The momentum parameter  $\mu$  is set consistently to 0.9. The approach is outlined in Algorithm 3, where the residual is computed, used to update the velocity of  $\mathbf{r}$ , then subsequently  $\mathbf{r}$  itself.

---

#### Algorithm 3 MGD( $\tilde{\mathbf{z}}_t, \mathbf{L}, T_r$ )

---

```

1: Initialization:  $\alpha = 10^{-5}, \eta = 5 \times 10^{-3}, \mu = 0.9, \mathbf{r} =$   

    $\alpha \mathbf{1}_r, \mathbf{v}_r = \mathbf{0}_r.$ 
2: for  $i = 0$  to  $T_r - 1$  do
3:    $\Delta \leftarrow \frac{4}{p}(\tilde{\mathbf{z}}_t - \mathbf{L}\mathbf{r})$ 
4:    $\mathbf{v}_r \leftarrow \mu \mathbf{v}_r - \eta\Delta; \quad \mathbf{r} \leftarrow \mathbf{r} + \mathbf{v}_r$ 
5: end for
6: return  $\mathbf{r}$ 
```

---

This implicitly eliminates  $\lambda_1$  from (5). To eliminate the dependency on the parameter  $\lambda_1$  from equation (3), we estimate the basis implicitly in the next subsection.

#### C. Estimate the subspace basis $\mathbf{L}$

Estimating  $\mathbf{L}$  requires minimization of the loss function penalized by the Frobenius norm of  $\mathbf{L}$  (optimization problem  $P_3$  (equation (6))). A standard matrix factorized gradient descent method [18] for matrix completion is insufficient, as it tends to converge to the nuclear norm of the matrix and is thus not directly applicable here. Addressing this

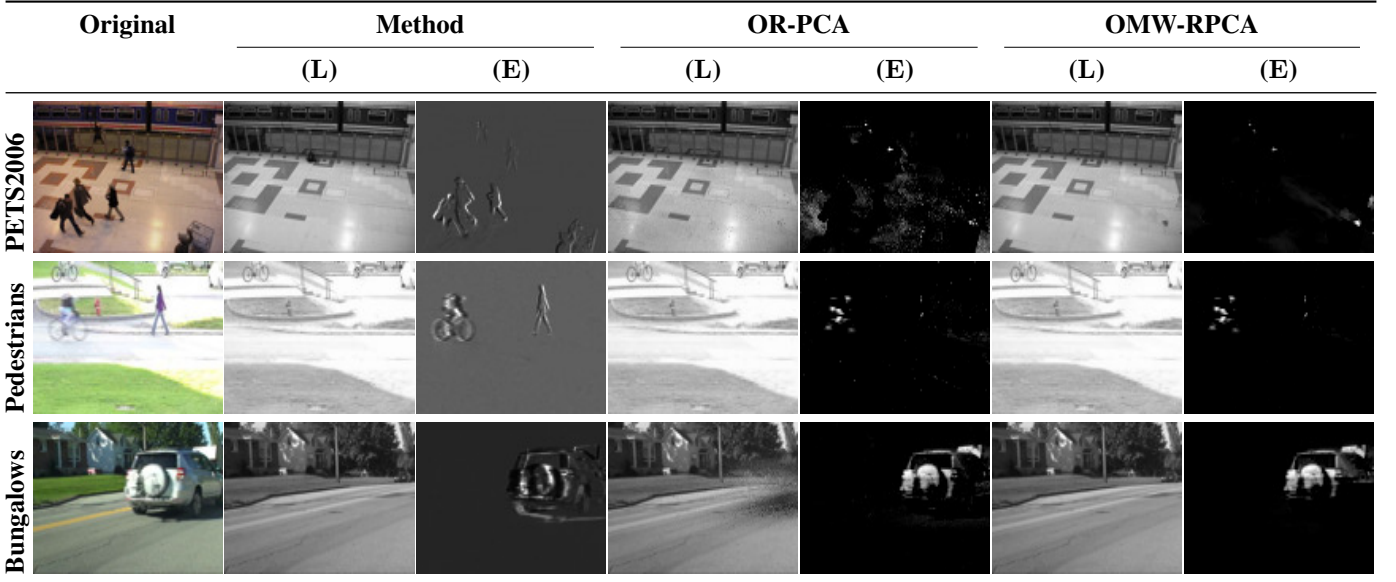


Fig. 1: Video surveillance in various datasets (top to bottom: PETS2006, Pedestrians, and Bungalows). Columns (left to right) illustrate: col. 1 – Original image, col. 2 & 3 – Low-rank background (L) and sparse foreground (E) components recovered by TF-ORPCA, col. 4 & 5 – L and E recovered by OR-PCA, col. 6 & 7 – L and E recovered by OMW-RPCA

challenge is a key novel aspect of TF-ORPCA. The proposed Algorithm 4 employs a unique and novel reparameterization  $\mathbf{L} = \mathbf{g}^{\odot 2} \mathbf{1}_r \odot \mathbf{V}$ , where  $\mathbf{g} \in \mathbb{R}^{p \times 1}$ , and  $\mathbf{V} \in \mathbb{R}^{p \times r}$ . The intuition behind parameterization is that it separates the control of the magnitude in the row  $\mathbf{g}$  and the direction of the basis in the element  $\mathbf{V}$ . This separation allows for refined control over the low-rank structure by implicitly balancing the magnitude of rows and the directional components of the basis, thereby mimicking the effect of the Frobenius norm regularization. The associated updates (lines 4-6) implicitly manage the basis structure, aiming to mimic the effect of  $\|\mathbf{L}\|_F^2$  without the dependence on the tuning parameter  $\lambda_1$  in equation (6). As with the previous algorithms, each element is individually updated at each iteration; the residual is used to update the parameters  $\mathbf{g}$  and  $\mathbf{V}$ , which then calculate  $\mathbf{L}$ . While rigorous theoretical guarantees for this novel algorithm are part of an ongoing investigation and future work, we emphasize its empirical effectiveness in the following section that incorporates this novel reparameterization.

---

**Algorithm 4** HPGGroupGrad( $\mathbf{z}_t, \mathbf{r}_t, T_L, \mathbf{L}$ )

---

- 1: **Initialization:**  $\eta = 5 \times 10^{-3}$ ,  $\mathbf{L}_0 = \mathbf{L}$ ,  $i = 0$
  - 2: **repeat**
  - 3:    $\Delta \leftarrow (\mathbf{z}_t - \mathbf{L} \mathbf{r}_t^\top) \mathbf{r}_t$
  - 4:    $\mathbf{g} \leftarrow \mathbf{g} - \frac{\eta}{p} (\Delta \odot (\mathbf{g} \mathbf{I}_r) \odot \mathbf{V}) \mathbf{I}_r^\top$
  - 5:    $\mathbf{V} \leftarrow \mathbf{V} - \frac{\eta}{p} \Delta \odot (\mathbf{g} \mathbf{I}_r)^{\odot 2}$
  - 6:    $\mathbf{L} \leftarrow (\mathbf{g}_i^{\odot 2} \mathbf{I}_r) \odot \mathbf{V}$
  - 7:    $i \leftarrow i + 1$
  - 8: **until**  $i = T_L$
  - 9:  $\mathbf{g}_0 \leftarrow \mathbf{g}$ ;  $\mathbf{v}_0 \leftarrow \mathbf{v}$
  - 10: **return**  $\mathbf{L}$
- 

## IV. SIMULATION RESULTS

### A. Synthetic Data Case Studies

For synthetic evaluations,  $\mathbf{X} = \mathbf{U} \mathbf{V}^\top$  is generated with  $n = 200$ , ambient dimension  $p = 80$ , where  $\mathbf{U}, \mathbf{V} \sim \mathcal{N}(0, \frac{1}{n})$ , and the intrinsic dimension of the subspace spanned by  $\mathbf{U}$  is  $r = 10$ . The observed samples are  $\mathbf{Z} = \mathbf{X} + \mathbf{E}$ , with  $\mathbf{E} \sim \mathcal{U}(-1000, 1000)$ , where a fraction ( $\rho = 0.01$ ) of its entries is non-zero. This configuration serves as **Case I** of our studies. For **Case II**, we use  $n = 1000$ ,  $p = 400$ ,  $r = 10$ , and  $\rho = 0.01$ . To compare the performance, we use Expressed Variance (EV) [24]. Higher EV indicates better recovery of the underlying low-rank structure. For both OR-PCA and OMW-RPCA  $\lambda_1, \lambda_2$  are set to  $1/\sqrt{p}$ , as designed by the corresponding authors. We also included results from carefully tuned parameters ( $\lambda_1 = \lambda_2 = 1$ ) to achieve optimal EV after a grid search of values from 0 to 1.2 in increments of 0.1. For OMW-RPCA, the initial data points are reserved for rank estimation, which explains the absence of metrics in the initial iterations in Fig. 2. Figures plot the average EV over 10 experiments.

The hyperparameters for the TF-ORPCA are set with initial values are  $m_0 = n_0 = r_0 = V_0 = 10^{-5}$ , and  $g_0 = 1$ . The learning rate is set to  $\eta_r = \eta_e = \eta_g = \eta_v = 5 \times 10^{-3}$ . The number of epochs,  $T_e, T_r$ , and  $T_L$  are determined by Equations (7)-(9) in the Appendix. As Fig. 2 demonstrates, all algorithms' performance steadily improves with more samples. Notably, the EV of the TF-ORPCA is consistently better than that of OR-PCA. We also observe that the TF-ORPCA converges to a performance level comparable to that of carefully tuned OR-PCA and OMW-RPCA with window size 15, without requiring any dataset-dependent parameter tuning. The plot for OR-PCA shows significant degradation in performance ( $\text{EV} \leq 0.4$ ), demonstrating that it is susceptible to regularization parameters. The high performance of tuned-

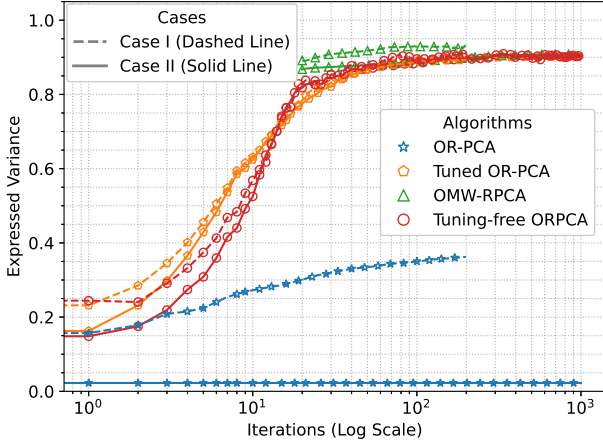


Fig. 2: Comparison of EV for four different OR-PCA methods.

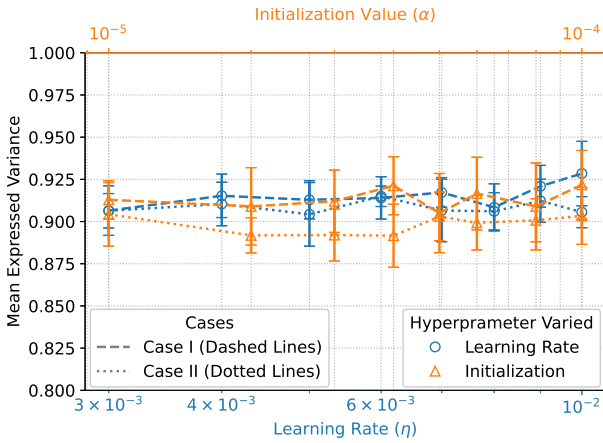


Fig. 3: Ablation Study of Tuning-Free OR-PCA

OR-PCA and OMW-RPCA is attributed to the careful tuning of the data-dependent parameters  $\lambda_1$ ,  $\lambda_2$ , and the window size. The better performance observed in TF-ORPCA stems from the adaptive nature of the IR introduced due to the different problem-specific reparameterizations used.

### B. Ablation Studies: Hyperparameter Sensitivity

To evaluate the robustness of TF-ORPCA, an ablation study was conducted on its hyperparameters. We specifically investigated the impact of the learning rate ( $\eta$ ) and the initialization value ( $\alpha$ ). We varied  $\eta$  across a range of values for the learning rate analysis while the initialization values were set to a fixed  $\alpha$ . In contrast, for the initialization value analysis,  $\alpha$  was varied with a fixed  $\eta$ . Fig. 3 demonstrates the remarkable stability and insensitivity of the algorithm to variations in both the learning rate and initialization values within the evaluated ranges, suggesting inherent robustness. More detailed information on these ablation studies can be found in Appendix.

### C. Real Dataset

Surveillance video is an excellent candidate for studying OR-PCA, where the background is the slow-changing low-rank component and the foreground corresponds to sparse outliers. A tuning-free approach is especially useful in these diverse, often unpredictable environments, as it eliminates

the need for manual parameter adjustments. For comparison, the OR-PCA and OMW-RPCA baselines were run with their typical default parameters,  $\lambda_1 = \lambda_2 = 1/\sqrt{p}$ . Fig. 1 illustrates the low-rank matrix and the sparse outlier recovery for the PETS2006, Pedestrians, and Bungalows datasets from the change detection dataset. The hyperparameters are kept the same across all datasets:  $\alpha = 10^{-5}$ ,  $\eta = 5 \times 10^{-3}$ , and epochs ( $T_e$ ,  $T_r$ , and  $T_L$ ) determined by Equations (7)-(9) in the Appendix. The images are resized from  $240 \times 360$  to  $48 \times 72$  to accommodate the algorithms.

The estimation of the low-rank matrix and the sparse outliers using TF-ORPCA is clear and exhibits minimal shadowing in the recovered low-rank matrix for all datasets. The results for OR-PCA (columns 4 and 5 of Fig. 1) highlight limitations in its consistent performance across datasets. Specifically, while low-rank recovery (column 4) appears satisfactory for the Pedestrians dataset, considerable background shadowing is evident in the Bungalows dataset, particularly around the estimated vehicle. The PETS2006 dataset exhibits undesirable gray patches in its low-rank recovery. Despite successful outlier extraction (column 5) in the Bungalows dataset, the quality of outlier recovery in the Pedestrians and PETS2006 datasets is compromised, with foreground objects appearing as significant noise rather than clear detections.

The results for OMW-RPCA (columns 6 and 7) demonstrate effective low-rank recovery and outlier detection for the Bungalows dataset and show proper low-rank estimation for the Pedestrians dataset. While the low-rank estimation for the PETS2006 dataset is generally good, it exhibits a minor estimation error spanning a few pixels. Furthermore, outlier detection for both the Pedestrians and PETS2006 datasets is poor, with a complete lack of distinct detections. Together, these observations for OR-PCA and OMW-RPCA strongly suggest that their performance is highly data sensitive, necessitating meticulous parameter tuning for each specific dataset. TF-ORPCA eliminates this need by using consistent hyperparameters across datasets, a robustness that is particularly advantageous in real-world scenarios where ground-truth or validation data for parameter selection are unavailable.

## V. CONCLUSION

We introduced tuning-free OR-PCA, which leverages implicit regularization to eliminate the regularization parameters. Our approach employs three problem-specific IR techniques to implicitly promote sparsity and a low-rank structure : (a) a modified gradient descent for an implicit  $\ell_1$ -regularizer, (b) an early-stopped momentum gradient descent for implicit  $\ell_2$ -regularizer, and (c) a novel reparameterization estimates the subspace basis that implicitly regularizes the Frobenius norm. Unlike traditional OR-PCA, which requires fine-tuning regularization parameters, our algorithm is relatively insensitive to the choice of its parameters, and hence, does not require extensive tuning. This enables OR-PCA to be applied to real-world applications, such as video surveillance, where traditional tuning-dependent approaches are often ineffective. Our method clearly extracts foreground and background components without the artifacts, such as shadowing or gray patches, often seen with traditional approaches.

## APPENDIX

This section provides the early stopping criteria used in the algorithms presented in the main paper. The alternating optimization loop in Algorithm 1 runs for a maximum of  $T_0 = 50$  iterations. Each sub-optimization for  $\mathbf{e}_t$ ,  $\mathbf{r}_t$ , and  $\mathbf{L}$  (Algorithms 2, 3, and 4) is performed for a fixed number of epochs, denoted as  $T_e$ ,  $T_r$ , and  $T_L$ , respectively. For algorithm 2, the maximum number of iterations,  $T_e$ , is set according to the derivation in [23] as:

$$T_e = \frac{15}{32}n \log_2 \left( \frac{\max(|\tilde{\mathbf{z}}_t|) - \alpha^2}{\eta^2 \epsilon} \right), \quad (7)$$

where  $n$  is the number of samples,  $\alpha$  is the initialization constant,  $\eta$  is the learning rate, and  $\epsilon$  is the expected accuracy between updates and the oracle value. Similarly, for algorithms 3 and 4, the maximum number of iterations for  $T_r$  is set to:

$$T_r = \frac{15}{32}r \log_2 \left( \frac{\max(|\tilde{\mathbf{z}}_t|) - \alpha^2}{\eta^2 \epsilon} \right), \quad (8)$$

$$T_L = \frac{15}{32}nr \log_2 \left( \frac{\max(|\mathbf{z}_t|) - \alpha^2}{\eta^2 \epsilon} \right). \quad (9)$$

This duration is determined similarly to  $T_e$ , considering the dimensions  $n$  and  $r$  of the matrices involved.

This section presents further experimental results that complement those reported in the main paper.

#### A. Ablation Study: Sensitivity to hyperparameters

This section provides further details on the algorithm's hyperparameter sensitivity. The same synthetic datasets as in Cases I and II are utilized for the learning rate analysis. All initialization values were consistently set to  $\alpha = 10^{-5}$ . A single learning rate was uniformly applied across all constituent subalgorithms during optimization. We varied  $\eta$  across eight distinct values ranging from  $3 \times 10^{-3}$  to  $10^{-2}$ . Fig. 3 presents the mean EV obtained from 10 independent experiments for each tested learning rate and initialization value.

Fig. 3 distinctly shows that the algorithm's performance, in terms of the mean EV, remains remarkably stable and largely insensitive to variations in both the learning rate and the initialization value within the evaluated range. Specifically, for the initialization value, this insensitivity holds, provided the value is not excessively small, as extremely low initializations can lead to stagnation in gradient descent methods utilizing Hadamard reparameterization (e.g., Algorithm 2 for sparse noise estimation). For both studies, the y-axes were zoomed in for clarity, and the error bars depict the standard deviation of 10 experiments, further substantiating consistent performance. Collectively, these studies reveal a strong insensitivity of the algorithm to the precise choice of initialization values and learning rates within the evaluated ranges, suggesting inherent robustness.

## REFERENCES

- [1] V. Menon and S. Kalyani, "Structured and unstructured outlier identification for robust PCA: A fast parameter free algorithm," *IEEE Transactions on Signal Processing*, vol. 67, 2019.
- [2] E. J. Candès, X. Li, Y. Ma, and J. Wright, "Robust principal component analysis?" *Journal of the ACM (JACM)*, vol. 58, no. 3, 2011.
- [3] J. Fan, L. Ding, Y. Chen, and M. Udell, "Factor group-sparse regularization for efficient low-rank matrix recovery," *Advances in neural information processing systems*, vol. 32, 2019.
- [4] G. Mateos and G. B. Giannakis, "Robust pca as bilinear decomposition with outlier-sparsity regularization," *IEEE Transactions on Signal Processing*, vol. 60, no. 10, pp. 5176–5190, 2012.
- [5] N. Vaswani, T. Bouwmans, S. Javed, and P. Narayanamurthy, "Robust subspace learning: Robust pca, robust subspace tracking, and robust subspace recovery," *IEEE signal processing magazine*, vol. 35, no. 4, pp. 32–55, 2018.
- [6] J. Zhan, B. Lois, H. Guo, and N. Vaswani, "Online (and offline) robust PCA: Novel algorithms and performance guarantees," in *Artificial intelligence and statistics*, 2016.
- [7] J. Feng, H. Xu, and S. Yan, "Online robust PCA via stochastic optimization," *Advances in neural information processing systems*, vol. 26, 2013.
- [8] Z. Li, Y. Wang, Q. Zhao, S. Zhang, and D. Meng, "A tensor-based online rpca model for compressive background subtraction," *IEEE Transactions on Neural Networks and Learning Systems*, vol. 34, no. 12, pp. 10668–10682, 2022.
- [9] W. Xiao, X. Huang, F. He, J. Silva, S. Emrani, and A. Chaudhuri, "Online robust principal component analysis with change point detection," *IEEE Transactions on Multimedia*, vol. 22, pp. 59–68, 2019.
- [10] Q. Zhang, S. Li, J. Duan, J. Qin, and Y. Zhou, "Moving object detection method based on the fusion of online moving window robust principal component analysis and frame difference method," *Neural Processing Letters*, vol. 56, no. 2, p. 55, 2024.
- [11] O. Pulpito, N. Acito, M. Diani, G. Ferri, R. Grasso, and D. Zissis, "Saliency-aided online rpca for moving target detection in infrared maritime scenarios," *Sensors*, vol. 23, no. 14, p. 6334, 2023.
- [12] J. He, L. Balzano, and A. Szlam, "Incremental gradient on the grassmannian for online foreground and background separation in subsampled video," in *2012 IEEE Conference on Computer Vision and Pattern Recognition*, 2012.
- [13] P. Narayanamurthy and N. Vaswani, "Provable dynamic robust pca or robust subspace tracking," *IEEE Transactions on Information Theory*, vol. 65, no. 3, pp. 1547–1577, 2018.
- [14] T. Zhu and J. Shen, "Residual-based sampling for online outlier-robust pca," in *International Conference on Machine Learning*. PMLR, 2022, pp. 27591–27611.
- [15] C. Zhang, S. Bengio, M. Hardt, B. Recht, and O. Vinyals, "Understanding deep learning (still) requires rethinking generalization," *Communications of the ACM*, vol. 64, 2021.
- [16] L. Prechelt, "Early stopping-but when?" in *Neural Networks: Tricks of the trade*, 2002.
- [17] L. Ziyin, M. Wang, and L. Wu, "Loss symmetry and noise equilibrium of stochastic gradient descent," *arXiv preprint arXiv:2402.07193*, 2024.
- [18] S. Gunasekar, B. E. Woodworth, S. Bhojanapalli, B. Neyshabur, and N. Srebro, "Implicit regularization in matrix factorization," *Advances in neural information processing systems*, vol. 30, 2017.
- [19] T. Vaskevicius, V. Kanade, and P. Rebeschini, "Implicit regularization for optimal sparse recovery," *Advances in Neural Information Processing Systems*, vol. 32, 2019.
- [20] L. Wang, Z. Fu, Y. Zhou, and Z. Yan, "The implicit regularization of momentum gradient descent in overparametrized models," in *Proceedings of the AAAI Conference on Artificial Intelligence*, vol. 37, no. 8, 2023.
- [21] J. Li, T. V. Nguyen, C. Hegde, and R. K. Wong, "Implicit regularization for group sparsity," *arXiv preprint arXiv:2301.12540*, 2023.
- [22] B. Recht, M. Fazel, and P. A. Parrilo, "Guaranteed minimum-rank solutions of linear matrix equations via nuclear norm minimization," *SIAM review*, vol. 52, no. 3, pp. 471–501, 2010.
- [23] J. Li, T. Nguyen, C. Hegde, and K. W. Wong, "Implicit sparse regularization: The impact of depth and early stopping," *Advances in Neural Information Processing Systems*, vol. 34, 2021.
- [24] H. Xu, C. Caramanis, and S. Mannor, "Principal component analysis with contaminated data: The high dimensional case," *arXiv preprint arXiv:1002.4658*, 2010.